

Two-Dimensional Janus GePAs Monolayer: A Direct-Band-Gap Semiconductor with High and Anisotropic Mobility for Efficient Photocatalytic Water Splitting

D. H. Ozbey¹,^{*} M. E. Kilic,² and E. Durgun^{1,*}

¹UNAM—National Nanotechnology Research Center and Institute of Materials Science and Nanotechnology, Bilkent University, Ankara 06800, Turkey

²Computational Science Research Center, Korea Institute of Science and Technology, Seoul 02792, Republic of Korea

(Received 6 August 2021; revised 17 February 2022; accepted 18 February 2022; published 15 March 2022)

Two-dimensional (2D) materials with suitable electronic and optical properties offer various possibilities for photocatalytic applications. Although various 2D materials have hitherto been specified as adequate candidates, materials with high photocatalytic efficiency for water splitting are still minimal. In this study, we predict a 2D Janus GePAs monolayer and examine its capability for photocatalytic water splitting by performing first-principles calculations. The GePAs monolayer is shown to possess robust dynamic and thermal stability. The direct electronic band gap in the visible region and band-edge positions of the strain-free and strained monolayers are revealed to be convenient for redox reactions in wide pH ranges. The low recombination probability of charge carriers ensured by high and anisotropic carrier mobility enhances the material's photocatalytic potential. Optical response calculations, including many-body interactions, indicate significant optical absorption capacity in the UV-visible range. Furthermore, low exciton binding energy facilitates dissociation into free electrons and holes, promoting photocatalytic reactions. Our study suggests that the GePAs monolayer is an ideal and remarkably promising material to be utilized in visible-light-driven photocatalytic applications.

DOI: [10.1103/PhysRevApplied.17.034043](https://doi.org/10.1103/PhysRevApplied.17.034043)

I. INTRODUCTION

Since the early years of the two-dimensional (2D) materials era, noteworthy advancements have been made in the discovery of post-graphene 2D nanostructures [1–5]. Among these superior materials, group IV-V compounds with formula MX ($M = \text{C, Si, Ge, Sn, Pb}$; $X = \text{N, P, As, Sb, Bi}$) have attracted growing attention and have been intensively investigated both theoretically and experimentally [6–9]. A subset of this class (SiP, SiAs, GeP, and GeAs) in bulk form belongs to the van der Waals (vdW) layered materials family with orthorhombic ($Cmc2_1$ for SiP) or monoclinic ($C2/m$ for GeP, GeAs, and SiAs) symmetries [10]. Generally, owing to the possibility of mechanical exfoliation, the realization of a vdW layered system can be regarded as pioneering work for the isolation of 2D materials. For this reason, the fabrication of bulk single crystals of group IV monpnictides has made these materials even more attractive from a scientific point of view [10]. Accordingly, few-layer SiP nanoflakes have been successfully obtained by mechanical exfoliation methods, and the anisotropic nonlinear optical properties have been anticipated to represent great potential for

future photonic integrated circuits and quantum chips [11]. Lately, following the synthesis of SiAs nanosheets, the production of a field-effect transistor and photodetector devices have been demonstrated. It has been shown that fabricated photodetector devices offer high photosensitivity with a strong anisotropy in the UV-visible domain [12]. Moreover, GeP nanoflakes have been synthesized from bulk, and photodetectors with highly anisotropic electronic transport and photoresponsivity have been realized [13,14]. Based upon the same production procedure, Wang *et al.* have reported a 2D GeP-based photonic device in which they exploited the strong nonlinear optical properties of GeP nanoflakes [15]. Likewise, few-layered GeAs nanosheets have been synthesized successfully, and a GeAs-based photoanode has been characterized as a promising candidate for high-performance optoelectronic nanodevices [16].

By considering the experimental progress on the group IV-V family, researchers have concentrated significantly on 2D Ge-based binary structures due to their superior stability, Earth abundance, distinct anisotropic properties, and tunable band gaps [17–24]. Predominantly owing to their low symmetry and having different bonding types along with different directions, GeP and GeAs systems in monolayer form have been predicted to exhibit anisotropic

*durgun@unam.bilkent.edu.tr

electronic, mechanical, and optical absorption characteristics. For instance, these semiconductors possess wide band gaps falling into the visible transmittance range with values of 2.08 eV (direct) and 2.31 eV (indirect) estimated by hybrid functional calculations, respectively [8]. Moreover, the anisotropic absorption coefficient of GeP and GeAs single layers has been found to be higher compared with those of SiP and SiAs, and they have been suggested as promising candidates for solar water splitting [25].

Even though structures obtained by top-down strategies encompass a significant portion of the field of 2D materials, synthetically produced monolayers have been realized with experimental endeavors, as well [26–28]. One of the intriguing derivatives of them are Janus monolayers designed by substituting all atoms at one side of their binary counterpart with a different atom. Due to the breaking of out-of-plane mirror symmetry by adding a third element, Janus monolayers can exhibit fascinating physical properties, or their capabilities can be enhanced concerning the prior structure. The realization of ternary MoSSe monolayers and their intrinsic vertical piezoelectric response underline the great potential of Janus materials [29,30]. Apart from transition metal dichalcogenides, various Janus structures including silicon- and germanium-based systems have been predicted, and their potential usage for diverse applications has been investigated [31–35].

In this work, motivated by the aforementioned experimental and theoretical advancements and considering unique properties of GeP and GeAs systems, we design a Janus GePAs monolayer and reveal its effective photocatalytic performance. Firstly, we obtain the ground-state configuration of the GePAs monolayer and examine its dynamical, thermal, and mechanical stability. Subsequent to confirmation of the stability, we investigate the electronic properties with or without applied strain and determine the band-edge positions concerning the redox potential of water. Next, we compute the carrier effective mass and mobility reflecting the ability to inhibit recombination of electron-hole pairs. Lastly, we explore the optical response of the GePAs monolayer, taking into account many-body interactions.

II. METHODOLOGY

All calculations in this paper are performed with the Vienna *ab initio* simulation package [36,37] based on density functional theory (DFT). To approximate the exchange-correlation functional, the generalized gradient approximation with Perdew-Burke-Ernzerhof (GGA-PBE) [38] formalism is selected. The projected augmented wave method with a plane-wave cutoff energy of 530 eV is used to take into account the ion-electron interactions [39]. The Brillouin zone is sampled by a Γ -centered $24 \times 4 \times 1$ k -point mesh within the Monkhorst-Pack scheme [40].

To avoid artificial interactions, vacuum space is set to 15 Å, which is tested to be adequate. The Grimme method (DFT-D3) is applied to describe vdW interactions [41]. The lattice parameters and atomic positions are relaxed until forces on the atoms are less than 0.01 eV/Å and the energy difference between two successive steps is smaller than 10^{-5} eV. A well-known fact being that the GGA-PBE formalism underestimates the electronic band gaps, the Heyd-Scuseria-Ernzerhof (HSE06) hybrid functional approach is implemented to calculate a more accurate electronic band gap and band edges [42,43]. The effect of spin-orbit coupling (SOC) is taken into consideration with the fully unconstrained noncollinear magnetic method [44] for both PBE and HSE06 levels. The charge transfer analysis among the atoms is performed by using the Bader technique [45,46]. Using an $8 \times 1 \times 1$ supercell, the phonon spectrum is obtained by the small displacement method implemented in the PHONOPY package [47]. The thermal stability is studied by performing *ab initio* molecular dynamics (AIMD) simulations during a total of 9-ps simulation time with 1-fs time steps. To examine the optical response of the system beyond the independent-particle approach, single-shot G_0W_0 approximation [48] is employed, and excitonic effects are treated by solving the Bethe-Salpeter equation (BSE) [49] within the Tamm-Dancoff approximation. For the G_0W_0 calculations, a k -point set of $20 \times 3 \times 1$ and cutoff energy of 320 eV are used, and the number of bands is increased to 144. It should also be noted that a dense k -point grid is required to precisely calculate the exciton binding energy [50,51].

III. RESULTS AND DISCUSSION

Inspired by the recent experimental studies of ternary monolayers and the synthesized 2D GeP and GeAs configurations, the GePAs structure is designed by substituting the topmost layer of the 2D GeP [8] with arsenic atoms. Following this substitution, the Janus GePAs monolayer is characterized by the monoclinic C_s point group (Cm space group) with broken symmetries including rotation and inversion symmetries with respect to GeP and GeAs counterparts, which belong to the C_{2h} point group ($C2/m$ space group). As illustrated in Fig. 1(a), the rectangular unit cell consists of 12 germanium, 6 phosphorus, and 6 arsenic atoms, and the optimized lattice constants are $a = 3.70$ Å, $b = 21.59$ Å with inclusion of vdW correction ($a = 3.74$ Å, $b = 21.86$ Å without vdW correction) [31]. Our Bader charge analysis indicates that shared electrons are distributed in accordance with the electronegativity difference of respective atoms, as shown in Fig. 1(b).

Bond strength is an important parameter regarding the thermal stability of a material, which can be reflected by the cohesive energy. The cohesive energy per atom (E_{coh})

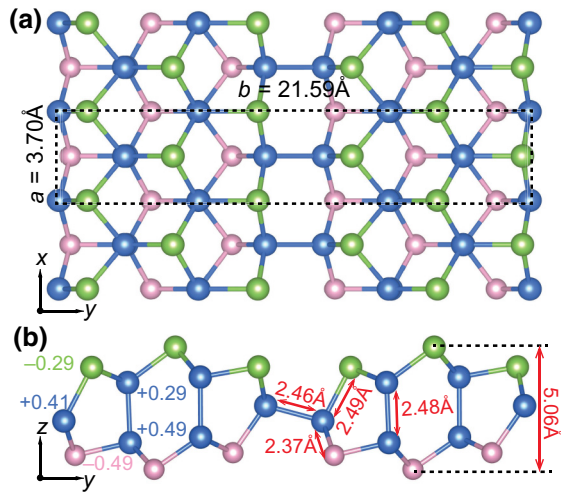


FIG. 1. (a) Top and (b) side views of Janus GePAs monolayer. The unit cell is marked by a dashed black rectangle. Layer thickness and bond lengths (red) are denoted and donated (+) and accepted (−) charges are shown with relevant color codes. Germanium, phosphorus, and arsenic atoms are presented as blue, pink, and green spheres, respectively.

of GePAs monolayer is calculated as

$$E_{\text{coh}} = \frac{E_{\text{GePAs}} - 12 \times E_{\text{Ge}} - 6 \times E_{\text{P}} - 6 \times E_{\text{As}}}{24}, \quad (1)$$

where E_{GePAs} is the total energy of the GePAs monolayer and E_{Ge} , E_{P} , and E_{As} are the single-atom energies of the respective elements. According to our calculations, E_{coh} of GePAs (3.73 eV/atom) is between those of the GeP (3.84 eV/atom) and GeAs (3.62 eV/atom) monolayers. Considering the experimental realization of 2D GeP and GeAs, E_{coh} indicates that the Janus GePAs configuration is energetically favorable. The elastic constants (C_{ij}), which are obtained by fitting the strain-energy curve (see Fig. S1 within the Supplemental Material [52]), satisfy the Born-Huang criteria [53] ($C_{11}C_{22} - C_{12}^2 > 0$ and $C_{66} > 0$) and confirm the mechanical stability of the GePAs monolayer. Albeit the structural optimization and Born-Huang criteria provide essential conditions, they do not ensure dynamical stability. Therefore, phonon spectra analysis is performed, and the lack of imaginary modes in the phonon band structure, as shown in Fig. 2(a), demonstrates that the GePAs monolayer is dynamically stable [31]. We further analyze the high-temperature stability by carrying out AIMD simulations, in which the monolayer is kept at 200, 400, and 600 K. Resultant snapshots demonstrate no bond breaking, and the total energy fluctuates around a certain value without a distinct drop during the simulation for the considered temperatures, as given in Fig. 2. These findings indicate that the GePAs monolayer can maintain its crystalline form even at elevated temperatures.

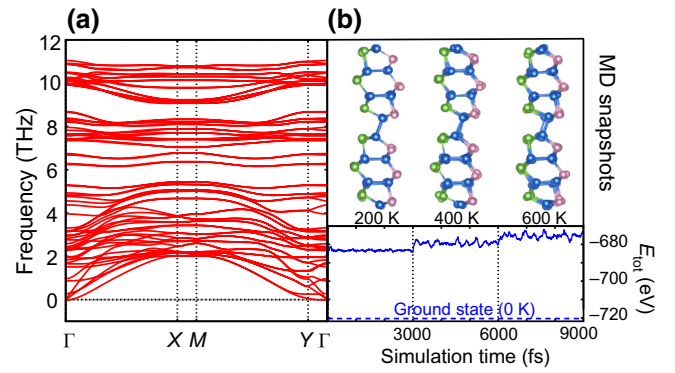


FIG. 2. (a) Phonon dispersion spectra of GePAs monolayer. (b) The evolution of total energy during the AIMD simulations (lower panel) and snapshots of the monolayer from side view at the end of each 3 ps (upper panel). The ground-state energy at 0 K is displayed by the dashed blue line.

Having demonstrated its stability, we proceed to our examination with the electronic properties of the monolayer. The electronic band structures of the GePAs monolayer calculated at the level of GGA PBE and HSE06 with the inclusion of SOC are given in Fig. 3 (see Fig. S2 within the Supplemental Material [52] for electronic band structures without SOC). Attaining accurate band structures is a crucial step to characterize the electronic properties. Although the system possesses an indirect band gap at the level of PBE and PBE+SOC [31], the precise HSE06+SOC calculations suggest that the GePAs monolayer is a direct semiconductor with a 2.21-eV band gap ($E_g^{\text{HSE06+SOC}}$) superior to its parent binary counterparts. Different dispersion profiles of valence and conduction bands close to the Fermi level can induce a high degree of in-plane anisotropy to electronic transport properties. The projected density of states (PDOS) of the GePAs monolayer is also given in

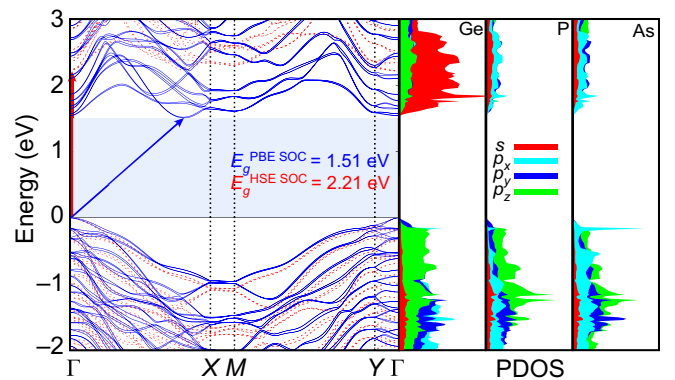


FIG. 3. The electronic band structure and PDOS of GePAs monolayer. The results for PBE+SOC and HSE06+SOC are shown with solid blue and dashed red lines, respectively. The Fermi level is set to zero.

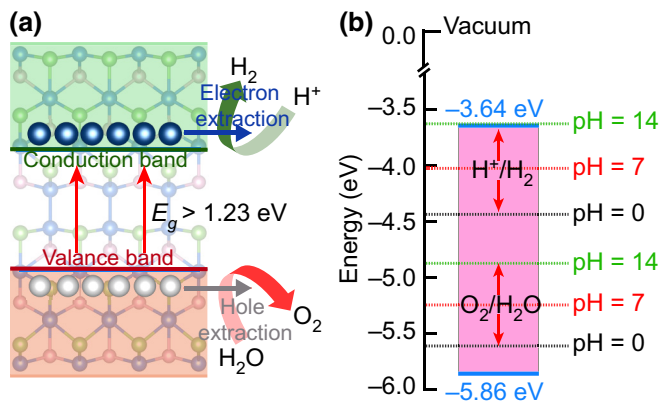


FIG. 4. (a) Representation of water-splitting process using a semiconductor photocatalyst. (b) Band-edge positions (VBM and CBM) of GePAs monolayer with respect to vacuum level. The redox potentials of water splitting are shown with black, red, and green dashed lines.

Fig. 3. The main contribution to conduction band minimum (CBM) comes from s orbitals of Ge atoms, while valence band maximum (VBM) is mostly composed of p_z orbitals of Ge, P, and As atoms. As illustrated in Fig. 4(a), a semiconductor with a band gap larger than 1.23 eV, which is the minimum Gibbs free energy required to split water, has the potential to be exploited as a photocatalyst. Even though numerous semiconductors meet the band-gap criterion, their band alignments with respect to the redox potential of the water are not viable for photocatalytic applications. To test the mentioned fundamental requirement for photocatalytic water splitting, band-edge positions are aligned with respect to the vacuum level. As depicted in Fig. 4(a), the energy levels of VBM (-5.86 eV) and CBM (-3.64 eV) of GePAs perfectly fit the redox potential of water. It is important to note that a competent catalyst should also operate in a wide pH range

[31,54]. The redox potential of water splitting increases with pH, given with the Nernst equation [55]: $E_{\text{H}^+/\text{H}_2} = (-4.44 + \text{pH} \times 0.059)$ eV and $E_{\text{O}_2/\text{H}_2\text{O}} = (-5.67 + \text{pH} \times 0.059)$. As demonstrated in Fig. 4(b), $E_g^{\text{HSE SOC}}$ of the GePAs monolayer completely covers both the oxidation potential of $\text{O}_2/\text{H}_2\text{O}$ and the reduction potential of H^+/H_2 throughout the full pH range, from pH = 0 (acidic) to pH = 14 (basic). This suggests that the GePAs monolayer is photocatalytically active for simultaneous production of hydrogen and oxygen even in extreme conditions.

Considering realistic applications, a semiconductor photocatalyst that maintains its functionality under strain is highly desirable. Therefore, we examine the band-gap alteration and band alignment of the GePAs monolayer with respect to applied uniaxial strain (in x and y directions) and biaxial strain. Figure 5 exhibits the variation of E_g^{HSE} with the band alignment of -2% to $+8\%$ strained monolayers. Remarkably, E_g^{HSE} values of 2D GePAs under all uniaxial and biaxial strains (except $+8\%$ biaxial strain) are larger than 1.23 eV, and related band-edge positions cover water redox potentials in wide pH ranges. These results indicate that the GePAs monolayer can operate under practical compressive and tensile strain levels. In this manner, it is also worth mentioning the mechanical response of the system in the elastic regime. The in-plane elastic modulus $Y^{2\text{D}}(\Theta)$, which is a measure of tensile stiffness, is computed as 84 and 62 N m^{-1} along x and y axes, and indicates the flexibility of the GePAs monolayer (see Fig. S3 within the Supplemental Material [52]). Having soft elastic constants is an advantage in terms of strain engineering without inducing fracture [56].

A promising semiconductor to be exploited for photocatalytic water splitting should not only possess overall suitability but also exhibit high efficiency. As spatially discrete electrons and holes perform redox activities separately during hydrogen reduction, $2\text{H}^+ + 2e^- \rightarrow \text{H}_2$, and oxidation, $\text{H}_2\text{O} + 2h^+ \rightarrow (1/2)\text{O}_2 + 2\text{H}^+$, reactions,

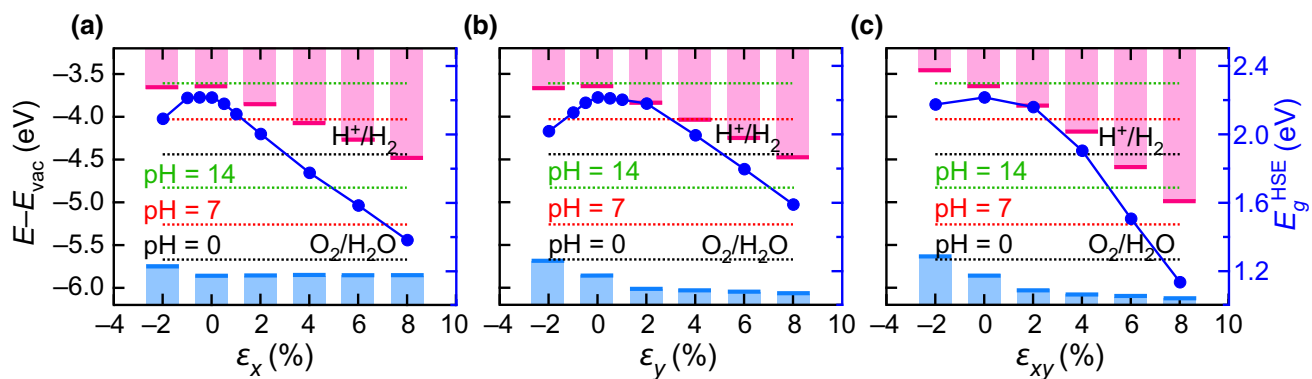


FIG. 5. HSE06 band gaps (blue dots) and band-edge positions for (a) uniaxial (x), (b) uniaxial (y), and (c) biaxial strains of GePAs monolayer with respect to the vacuum level under strain from -2% to $+8\%$ [negative (positive) numbers refer to compressive (tensile) strain]. The pink and blue bars represent the positions of the CBM and the VBM, respectively. The redox potentials of water splitting are shown as black, red, and green dashed lines.

TABLE I. Carrier effective mass m^* (m_0 is the mass of free electrons and m_d is the average effective mass) along Γ - X and Γ - Y directions, deformation potential constant E_d (eV), and carrier mobility μ ($\text{cm}^2 \text{V}^{-1} \text{s}^{-1}$) of GePAs monolayer along the x and y directions.

	m_x^*/m_0	m_y^*/m_0	m_d^*/m_0	E_d^x	E_d^y	μ_x	μ_y
electron	0.08	1.20	0.31	0.59	8.83	21.40×10^4	47.43
hole	0.30	0.37	0.33	0.30	7.82	20.13×10^4	182.62

a decrease in the recombination possibility of photogenerated charge carriers boosts the photocatalytic performance [56]. Recombination of free electrons and holes can efficiently be suppressed if the catalyst offers highly anisotropic transport of charge carriers [57]. To investigate the migration ability of carriers, effective mass (m^*) and carrier mobility (μ) are calculated along the x and y directions of the GePAs monolayer. The effective masses of electrons (m_e^*) and holes (m_h^*) are estimated by the quadratic fitting of the electronic band structure with the following expression: $m^* = \hbar[d^2E(k)/dk^2]^{-1}$, where \hbar is the reduced Planck constant, k is the wave vector, and $E(k)$ is the energy with respect to k . To obtain μ , we calculate the deformation potential constant E_d ; and using m^* , C , and E_d we get the room-temperature carrier mobility for x and y directions (μ_x and μ_y) by using the formula within the deformation potential theory [58]: $\mu = eh^3C/(2\pi)^3k_B T m^* m_d^2 E_d^2$, where $m_d = \sqrt{m_x^* m_y^*}$ is the average effective mass, C is the corresponding elastic constant, k_B is the Boltzmann constant, and T is the temperature in kelvin. Resultant values are summarized in Table I and details of estimation are given in Fig S4 within the Supplemental Material [52]. Taking the electronic band structure into account, the disparity in the curvature of the band dispersion throughout Γ - X and Γ - Y directions for both the lowest conduction band and the highest valence band is an indication of the anisotropic character of m^* and μ . The presence of light charge carriers along Γ - X direction with $m_{e,x}^* = 0.08m_0$ and $m_{e,y}^* = 0.30m_0$ stems from the available bonding environment of 2D GePAs in the x direction, and gives rise to extremely high mobilities with $\mu_{e,x} = 21.40 \times 10^4$ and $\mu_{h,x} = 20.13 \times 10^4 \text{ cm}^2 \text{V}^{-1} \text{s}^{-1}$, larger than the ultrahigh mobility of few-layered black phosphorus, which is shown to be $\mu = 2.60 \times 10^4$ theoretically and approximately $10^3 \text{ cm}^2 \text{V}^{-1} \text{s}^{-1}$ experimentally [59]. On the other hand, the horizontal Ge-Ge bond in the y direction behaves as a bottleneck for free electrons and holes. The different dispersion profiles regarding Γ - X direction and low values of corresponding carrier mobilities in the y direction can be attributed to this structural anisotropy. The details of calculation are shown in Fig S5 within the Supplemental Material [52]. Consequently, the ideal migration capability of the GePAs monolayer with strong anisotropy facilitates the photogenerated carriers' motion and, therefore, boosts the photocatalytic efficiency.

Since the primary strategy in visible-light-driven photocatalysis is to convert sunlight into chemical energy, the solar light absorption capacity of a photocatalyst plays a crucial role in improving efficiency. Moreover, weak exciton binding energy (E_b) enables charge carriers to be separated rapidly to improve the performance of the water-splitting process. To specify the optical absorption capability and exciton binding, we calculate the frequency-dependent imaginary dielectric function [$\epsilon(\omega) = \epsilon_1(\omega) + i\epsilon_2(\omega)$] (see Fig. S6 within the Supplemental Material [52]) and the optical absorption coefficient for incident light polarization along x ($\mathbf{E} \parallel x$) and y ($\mathbf{E} \parallel y$) directions by taking into account the electron-hole interactions by solving the BSE. It should be noted that the optical response of 2D systems can be strongly affected by excitonic features and many-body interactions should be taken into account [60–62]. The first prominent absorption peaks are observed in the middle part of the visible region, as shown in Fig. 6. The absorption spectrum shows that a significant portion of light can also be captured from the ultraviolet region and the anisotropic nature of the GePAs monolayer is much more pronounced in this region. Thus, the GePAs monolayer covers a broad absorption range with high absorbance (approximately 10^5 cm^{-1}) and can be

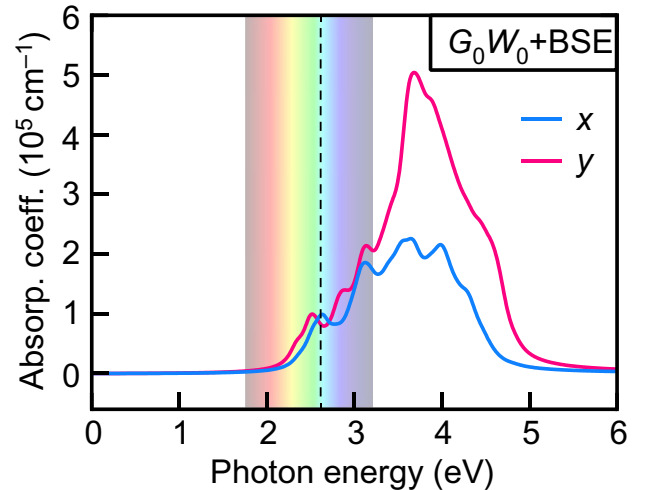


FIG. 6. Absorption coefficient for incident light polarization along the x (blue) and y (pink) directions. Energy range of visible light is given by the color spectrum in the plot. The band gap at the level of GW (E_g^{GW}) is denoted by the dashed line.

comparable with perovskite solar cells [63], supporting its superior properties in terms of water-splitting reaction. In addition, E_b is obtained with respect to E_g^{GW} and is found to be 85 meV (see Fig. S7 within the Supplemental Material [52]), which can be considered as weak in the family of 2D materials [64] and enhances the efficiency of the GePAs monolayer.

IV. CONCLUSION

In summary, motivated by recent experimental advancements in 2D GeP and GeAs materials, we design a Janus GePAs monolayer and reveal its unique properties within the scope of photocatalytic water splitting. We have shown that the GePAs monolayer is dynamically stable and can preserve its crystalline configuration even at high temperatures. The proposed system is a flexible, direct-band-gap semiconductor with high optical absorption in the visible to UV part of the spectrum. The band-edge position of the monolayer is adequate for redox reactions covering the entire pH range (from 0 to 14), indicating its potential usage in extreme conditions. Additionally, the GePAs monolayer can operate under applicable strain levels (-2% to $+8\%$). Anisotropic and significantly high mobility (approximately $10^5 \text{ cm}^2 \text{ V}^{-1} \text{ s}^{-1}$) and weak exciton binding herald notable performance of the GePAs monolayer as a photocatalyst. Our results demonstrate that the Janus GePAs monolayer has superior properties to those of its parent binary compounds and satisfies not only vital requirements of the water-splitting process but also offers high efficiency, thus revealing it as an ideal material to be utilized in photocatalytic applications.

ACKNOWLEDGMENTS

This work is supported by the Scientific and Technological Research Council of Turkey (TUBITAK) under Project No. 117F383. The calculations were performed at TUBITAK ULAKBIM, High Performance and Grid Computing Center (TR-Grid e-Infrastructure) and the National Center for High Performance Computing of Turkey (UHeM) under Grant No. 5007092019. M.E.K. acknowledges support from Brain Pool Program through the National Research Foundation of Korea (NRF) funded by the Ministry of Science and ICT (2020H1D3A1A02081517).

-
- [1] F. Ersan, D. Keçik, V. Özçelik, Y. Kadioglu, O. Ü. Aktürk, E. Durgun, E. Aktürk, and S. Ciraci, Two-dimensional pnictogens: A review of recent progresses and future research directions, *Appl. Phys. Rev.* **6**, 021308 (2019).
 [2] Y. Liu, N. O. Weiss, X. Duan, H.-C. Cheng, Y. Huang, and X. Duan, Van der waals heterostructures and devices, *Nat. Rev. Mater.* **1**, 16042 (2016).

- [3] F. A. Rasmussen, and K. S. Thygesen, Computational 2D materials database: Electronic structure of transition-metal dichalcogenides and oxides, *J. Phys. Chem. C* **119**, 13169 (2015).
 [4] P. Miró, M. Audiffred, and T. Heine, An atlas of two-dimensional materials, *Chem. Soc. Rev.* **43**, 6537 (2014).
 [5] Z. Lu, G. P. Neupane, G. Jia, H. Zhao, D. Qi, Y. Du, Y. Lu, and Z. Yin, 2D materials based on main group element compounds: Phases, synthesis, characterization, and applications, *Adv. Funct. Mater.* **30**, 2001127 (2020).
 [6] B. Özdamar, G. Özbal, M. N. Çınar, K. Sevim, G. Kurt, B. Kaya, and H. Sevinçli, Structural, vibrational, and electronic properties of single-layer hexagonal crystals of group IV and V elements, *Phys. Rev. B* **98**, 045431 (2018).
 [7] M. Ashton, S. B. Sinnott, and R. G. Hennig, Computational discovery and characterization of polymorphic two-dimensional IV-V materials, *Appl. Phys. Lett.* **109**, 192103 (2016).
 [8] A.-Q. Cheng, Z. He, J. Zhao, H. Zeng, and R.-S. Chen, Monolayered silicon and germanium monopnictide semiconductors: Excellent stability, high absorbance, and strain engineering of electronic properties, *ACS Appl. Mater. Interfaces* **10**, 5133 (2018).
 [9] S. Zhang, S. Guo, Y. Huang, Z. Zhu, B. Cai, M. Xie, W. Zhou, and H. Zeng, Two-dimensional SiP: An unexplored direct band-gap semiconductor, *2D Mater.* **4**, 015030 (2016).
 [10] C. Barreteau, B. Michon, C. Besnard, and E. Giannini, High-pressure melt growth and transport properties of SiP, SiAs, GeP, and GeAs 2D layered semiconductors, *J. Cryst. Growth* **443**, 75 (2016).
 [11] H. Sar, J. Gao, and X. Yang, 2D layered SiP as anisotropic nonlinear optical material, *Sci. Rep.* **11**, 6372 (2021).
 [12] D. Kim, K. Park, J. H. Lee, I. S. Kwon, I. H. Kwak, and J. Park, Anisotropic 2D SiAs for high-performance UV-visible photodetectors, *Small* **17**, 2006310 (2021).
 [13] L. Li, W. Wang, P. Gong, X. Zhu, B. Deng, X. Shi, G. Gao, H. Li, and T. Zhai, 2D GeP: An unexploited low-symmetry semiconductor with strong in-plane anisotropy, *Adv. Mater.* **30**, 1706771 (2018).
 [14] D. Kim, K. Park, F. Shojaei, T. T. Debela, I. S. Kwon, I. H. Kwak, J. Seo, J. P. Ahn, J. Park, and H. S. Kang, Thickness-dependent bandgap and electrical properties of GeP nanosheets, *J. Mater. Chem. A* **7**, 16526 (2019).
 [15] Z. Wang, J. Guo, Y. Zhang, J. Liu, J. S. Ponraj, S. C. Dhanabalan, T. Zhai, X. Liu, Y. Song, and H. Zhang, 2D GeP-based photonic device for near-infrared and mid-infrared ultrafast photonics, *Nanophotonics* **9**, 3645 (2020).
 [16] C. S. Jung, D. Kim, S. Cha, Y. Myung, F. Shojaei, H. G. Abbas, J. A. Lee, E. H. Cha, J. Park, and H. S. Kang, Two-dimensional GeAs with a visible range band gap, *J. Mater. Chem. A* **6**, 9089 (2018).
 [17] Y. Xu, H. Zhang, H. Shao, G. Ni, J. Li, H. Lu, R. Zhang, B. Peng, Y. Zhu, and H. Zhu *et al.*, First-principles study on the electronic, optical, and transport properties of monolayer α - and β -GeSe, *Phys. Rev. B* **96**, 245421 (2017).
 [18] X. Zhou, X. Hu, B. Jin, J. Yu, K. Liu, H. Li, and T. Zhai, Highly anisotropic GeSe nanosheets for phototransistors with ultrahigh photoresponsivity, *Adv. Sci.* **5**, 1800478 (2018).

- [19] J. Guo, Y. Liu, Y. Ma, E. Zhu, S. Lee, Z. Lu, Z. Zhao, C. Xu, S.-J. Lee, and H. Wu *et al.*, Few-layer GeAs field-effect transistors and infrared photodetectors, *Adv. Mater.* **30**, 1705934 (2018).
- [20] Z. Zhou, M. Long, L. Pan, X. Wang, M. Zhong, M. Blei, J. Wang, J. Fang, S. Tongay, and W. Hu *et al.*, Perpendicular optical reversal of the linear dichroism and polarized photodetection in 2D GeAs, *ACS Nano* **12**, 12416 (2018).
- [21] A. Grillo, A. Di Bartolomeo, F. Urban, M. Passacantando, J. M. Caridad, J. Sun, and L. Camilli, Observation of 2D conduction in ultrathin germanium arsenide field-effect transistors, *ACS Appl. Mater. Interfaces* **12**, 12998 (2020).
- [22] G. Dushaq and M. Rasras, Multilayer 2D germanium phosphide (GeP) infrared phototransistor, *Opt. Express* **29**, 9419 (2021).
- [23] Y. Yang, S.-C. Liu, Z. Li, D.-J. Xue, and J.-S. Hu, In-plane anisotropic 2D Ge-based binary materials for optoelectronic applications, *ChemComm* **57**, 565 (2021).
- [24] E. Jiang, X. Zhu, T. Ouyang, C. Tang, J. Li, C. He, C. Zhang, and J. Zhong, The thermoelectric properties of monolayer SiP and GeP from first-principles calculations, *J. Appl. Phys.* **126**, 185106 (2019).
- [25] B. Mortazavi, M. Shahrokhi, G. Cuniberti, and X. Zhuang, Two-dimensional SiP, SiAs, GeP and GeAs as promising candidates for photocatalytic applications, *Coatings* **9**, 522 (2019).
- [26] A. J. Mannix, B. Kiraly, M. C. Hersam, and N. P. Guisinger, Synthesis and chemistry of elemental 2D materials, *Nat. Rev. Chem.* **1**, 0014 (2017).
- [27] L. Wang, P. Hu, Y. Long, Z. Liu, and X. He, Recent advances in ternary two-dimensional materials: Synthesis, properties and applications, *J. Mater. Chem. A* **5**, 22855 (2017).
- [28] C. Zhang, Y. Nie, S. Sanvito, and A. Du, First-principles prediction of a room-temperature ferromagnetic janus VSSe monolayer with piezoelectricity, ferroelasticity, and large valley polarization, *Nano Lett.* **19**, 1366 (2019).
- [29] J. Zhang, S. Jia, I. Kholmanov, L. Dong, D. Er, W. Chen, H. Guo, Z. Jin, V. B. Shenoy, and L. Shi *et al.*, Janus monolayer transition-metal dichalcogenides, *ACS Nano* **11**, 8192 (2017).
- [30] A.-Y. Lu, H. Zhu, J. Xiao, C.-P. Chuu, Y. Han, M.-H. Chiu, C.-C. Cheng, C.-W. Yang, K.-H. Wei, and Y. Yang *et al.*, Janus monolayers of transition metal dichalcogenides, *Nat. Nanotechnol.* **12**, 744 (2017).
- [31] X. Li, K. Zhang, X. Zeng, N. Li, and J. Wang, Electronic and photochemical properties of hybrid binary silicon and germanium derived janus monolayers, *Phys. Chem. Chem. Phys.* **23**, 17502 (2021).
- [32] A. Kandemir and H. Sahin, Janus single layers of In_2SSe : A first-principles study, *Phys. Rev. B* **97**, 155410 (2018).
- [33] R. da Silva, R. Barbosa, R. R. Mancano, N. Duraes, R. B. Pontes, R. Miwa, A. Fazzio, and J. E. Padilha, Metal chalcogenides janus monolayers for efficient hydrogen generation by photocatalytic water splitting, *ACS Appl. Nano Mater.* **2**, 890 (2019).
- [34] R. Li, Y. Cheng, and W. Huang, Recent progress of janus 2D transition metal chalcogenides: From theory to experiments, *Small* **14**, 1802091 (2018).
- [35] M. Demirtas, M. J. Varjovi, M. M. Çiçek, and E. Durgun, Tuning structural and electronic properties of two-dimensional aluminum monochalcogenides: Prediction of janus $\text{Al}_2\text{XX}'$ (X/X' : O, S, Se, Te) monolayers, *Phys. Rev. Mater.* **4**, 114003 (2020).
- [36] G. Kresse and J. Hafner, Ab initio molecular dynamics for liquid metals, *Phys. Rev. B* **47**, 558 (1993).
- [37] G. Kresse and J. Hafner, Ab initio molecular-dynamics simulation of the liquid-metal–amorphous-semiconductor transition in germanium, *Phys. Rev. B* **49**, 14251 (1994).
- [38] J. P. Perdew, K. Burke, and M. Ernzerhof, Generalized Gradient Approximation Made Simple, *Phys. Rev. Lett.* **77**, 3865 (1996).
- [39] P. E. Blöchl, Projector augmented-wave method, *Phys. Rev. B* **50**, 17953 (1994).
- [40] H. J. Monkhorst and J. D. Pack, Special points for brillouin-zone integrations, *Phys. Rev. B* **13**, 5188 (1976).
- [41] S. Grimme, Semiempirical GGA-type density functional constructed with a long-range dispersion correction, *J. Comput. Chem.* **27**, 1787 (2006).
- [42] J. Heyd, G. E. Scuseria, and M. Ernzerhof, Hybrid functionals based on a screened coulomb potential, *J. Chem. Phys.* **118**, 8207 (2003).
- [43] A. V. Krukau, O. A. Vydrov, A. F. Izmaylov, and G. E. Scuseria, Influence of the exchange screening parameter on the performance of screened hybrid functionals, *J. Chem. Phys.* **125**, 224106 (2006).
- [44] D. Hobbs, G. Kresse, and J. Hafner, Fully unconstrained noncollinear magnetism within the projector augmented-wave method, *Phys. Rev. B* **62**, 11556 (2000).
- [45] R. Bader, 1997 polanyi award lecture why are there atoms in chemistry?, *Can. J. Chem.* **76**, 973 (1998).
- [46] G. Henkelman, A. Arnaldsson, and H. Jónsson, A fast and robust algorithm for bader decomposition of charge density, *Comput. Mater. Sci.* **36**, 354 (2006).
- [47] A. Togo and I. Tanaka, First principles phonon calculations in materials science, *Scr. Mater.* **108**, 1 (2015).
- [48] M. Shishkin and G. Kresse, Implementation and performance of the frequency-dependent g_w method within the paw framework, *Phys. Rev. B* **74**, 035101 (2006).
- [49] E. E. Salpeter and H. A. Bethe, A relativistic equation for bound-state problems, *Phys. Rev.* **84**, 1232 (1951).
- [50] M. Rohlfing and S. G. Louie, Electron-Hole Excitations in Semiconductors and Insulators, *Phys. Rev. Lett.* **81**, 2312 (1998).
- [51] D. Y. Qiu, H. Felipe, and S. G. Louie, Screening and many-body effects in two-dimensional crystals: Monolayer MoS_2 , *Phys. Rev. B* **93**, 235435 (2016).
- [52] See Supplemental Material at <http://link.aps.org/supplemental/10.1103/PhysRevApplied.17.034043> for additional details on variation of energy with strain, electronic band structures without spin-orbit coupling, mechanical properties, fitting steps (effective mass and mobility), and variation of complex dielectric function with photon energy and k -point grid.
- [53] M. Born and K. Huang, *Dynamical Theory of Crystal Lattices* (Clarendon press, Oxford, UK, 1954).
- [54] X. Zou, X. Huang, A. Goswami, R. Silva, B. R. Sathe, E. Mikmeková, and T. Asefa, Cobalt-embedded nitrogen-rich carbon nanotubes efficiently catalyze hydrogen evolution reaction at all pH values, *Angew. Chem.* **126**, 4461 (2014).

- [55] V. Chakrapani, J. C. Angus, A. B. Anderson, S. D. Wolter, B. R. Stoner, and G. U. Sumanasekera, Charge transfer equilibria between diamond and an aqueous oxygen electrochemical redox couple, *Science* **318**, 1424 (2007).
- [56] A. K. Singh, K. Mathew, H. L. Zhuang, and R. G. Hennig, Computational screening of 2D materials for photocatalysis, *J. Phys. Chem. Lett.* **6**, 1087 (2015).
- [57] Y. Xu, K. Xu, C. Ma, Y. Chen, H. Zhang, Y. Liu, and Y. Ji, Novel two-dimensional β -GeSe and β -SnSe semiconductors: Anisotropic high carrier mobility and excellent photocatalytic water splitting, *J. Mater. Chem. A* **8**, 19612 (2020).
- [58] J. Bardeen and W. Shockley, Deformation potentials and mobilities in non-polar crystals, *Phys. Rev.* **80**, 72 (1950).
- [59] J. Qiao, X. Kong, Z.-X. Hu, F. Yang, and W. Ji, High-mobility transport anisotropy and linear dichroism in few-layer black phosphorus, *Nat. Commun.* **5**, 4475 (2014).
- [60] M. Bernardi, C. Ataca, M. Palummo, and J. C. Grossman, Optical and electronic properties of two-dimensional layered materials, *Nanophotonics* **6**, 479 (2017).
- [61] D. Y. Qiu, H. Felipe, and S. G. Louie, Optical Spectrum of MoS₂: Many-Body Effects and Diversity of Exciton States, *Phys. Rev. Lett.* **111**, 216805 (2013).
- [62] T. Mueller and E. Malic, Exciton physics and device application of two-dimensional transition metal dichalcogenide semiconductors, *NPJ 2D Mater. Appl.* **2**, 29 (2018).
- [63] M. Shirayama, H. Kadowaki, T. Miyadera, T. Sugita, M. Tamakoshi, M. Kato, T. Fujiseki, D. Murata, S. Hara, and T. N. Murakami *et al.*, Optical Transitions in Hybrid Perovskite Solar Cells: Ellipsometry, Density Functional Theory, and Quantum Efficiency Analyses for CH₃NH₃PbI₃, *Phys. Rev. Appl.* **5**, 014012 (2016).
- [64] J. R. Schaibley, H. Yu, G. Clark, P. Rivera, J. S. Ross, K. L. Seyler, W. Yao, and X. Xu, Valleytronics in 2D materials, *Nat. Rev. Mat.* **1**, 16055 (2016).